Geophys. J. Int. (2000) **142,** 812–824

Magnetic polarity stratigraphy of Siwalik Group sediments of Karnali River section in western Nepal

Pitambar Gautam[1] and Yoshiki Fujiwara[2]

[1] *Central Department of Geology, Tribhuvan University, Kirtipur, Kathmandu, Nepal. E-mail: gautam@ptugeo.wlink.com.np*
[2] *Department of Earth and Planetary Sciences, Graduate School of Science, Hokkaido University,* N10 W8, *Sapporo* 060-0810, *Japan. E-mail: fujiwara@ep.sci.hokudai.ac.jp*

Accepted 2000 April 3. Received 2000 March 17; in original form 1999 May 26

SUMMARY

The remanent magnetization of siltstones and sandstones sampled at 476 levels/sites throughout a 3560 m thick molasse sequence belonging to the Siwalik Group (0–2015 m: Lower; 2015–3560 m: Middle) has been studied by stepwise thermal demagnetization. This section is exposed along the Karnali River in Nepal. The natural remanent magnetization (NRM) usually consists of two components: a viscous or thermoviscous component of recent field origin, and an ancient characteristic component (ChRM). The former component is of normal polarity and resides either in goethite (unblocking temperature <150 °C; resistant to AFD up to 150 mT) or in maghemite (unblocking temperature 150–400 °C). Goethite contributes up to 90 per cent of the total intensity in the finer variegated muddy samples belonging to the lower half of the section. Maghemite content is significant in the grey mud-free lithologies from the upper half of the section. The main component, unblocked in the high-temperature range (commonly 610–680 °C) and believed to reside in haematite, presumably of mostly detrital origin, represents a characteristic remanence (ChRM). The tilt-corrected ChRM directions at individual sites show antipodal clusters (ratio of normal- to reverse-polarity sites: 0.62), and yield mean inclinations recording significant inclination shallowing—a feature well recorded in the Siwaliks. This ChRM is interpreted to represent a largely primary detrital remanence.

The ChRM data from 430 sites yield the Karnali River magnetic polarity sequence, whose correlation with the geomagnetic polarity timescale (Cande & Kent 1995) suggests a depositional age of 16 Ma (younger than chron C5Cn.1n) to 5.2 Ma (around the top of chron C3r) for the 3560 m section sampled. Hence, the Karnali River exposes the oldest part of the Siwalik Group in Nepal. Estimates of the sediment accumulation rate (SAR) average to 32.9 cm kyr^{-1} for the 10.8 Myr time span of deposition.

Key words: foreland basin, goethite, haematite, Himalaya, magnetostratigraphy, Siwaliks.

INTRODUCTION

Magnetostratigraphic studies carried out during the last two decades of the Mio-Pliocene fluvial sediments of the Siwalik Group in the Sub-Himalaya of central Nepal have been useful in determining the depositional chronology through correlation of the magnetic polarity reversal record with the geomagnetic polarity timescales (Tokuoka *et al.* 1986; Appel *et al.* 1991; Harrison *et al.* 1993; Gautam & Appel 1994; Rösler *et al.* 1997; Rösler & Appel 1998; and a recent review by Gautam & Rösler 1999). The accumulated data set on polarity chronology from Nepal permits regional correlation of this sector with the Siwalik sections in India and Pakistan that have been well-dated through a combination of magnetostratigraphy and fission-track dating (see, for example, Keller *et al.* 1977; Barndt *et al.* 1978; Opdyke *et al.* 1979; Tauxe & Opdyke 1982; Johnson *et al.* 1982, 1983; Ranga Rao *et al.* 1988; Flynn *et al.* 1990; see also reviews by Opdyke 1990 and Burbank *et al.* 1996 and references therein). Owing to the absence of fossil- or isotope-constrained ages in the Siwaliks of Nepal, however, additional reversal records from the relatively thick (>1–2 km) sections in its eastern and western parts are required in order to gain an accurate overall chronological insight into the sedimentation and tectonic history of the central part of the fold-and-thrust foreland belt of the Himalaya.

In this paper, we present a new magnetic polarity stratigraphy for a 3560 m thick sedimentary column of Lower and Middle Siwaliks exposed along the Karnali River (KR). The

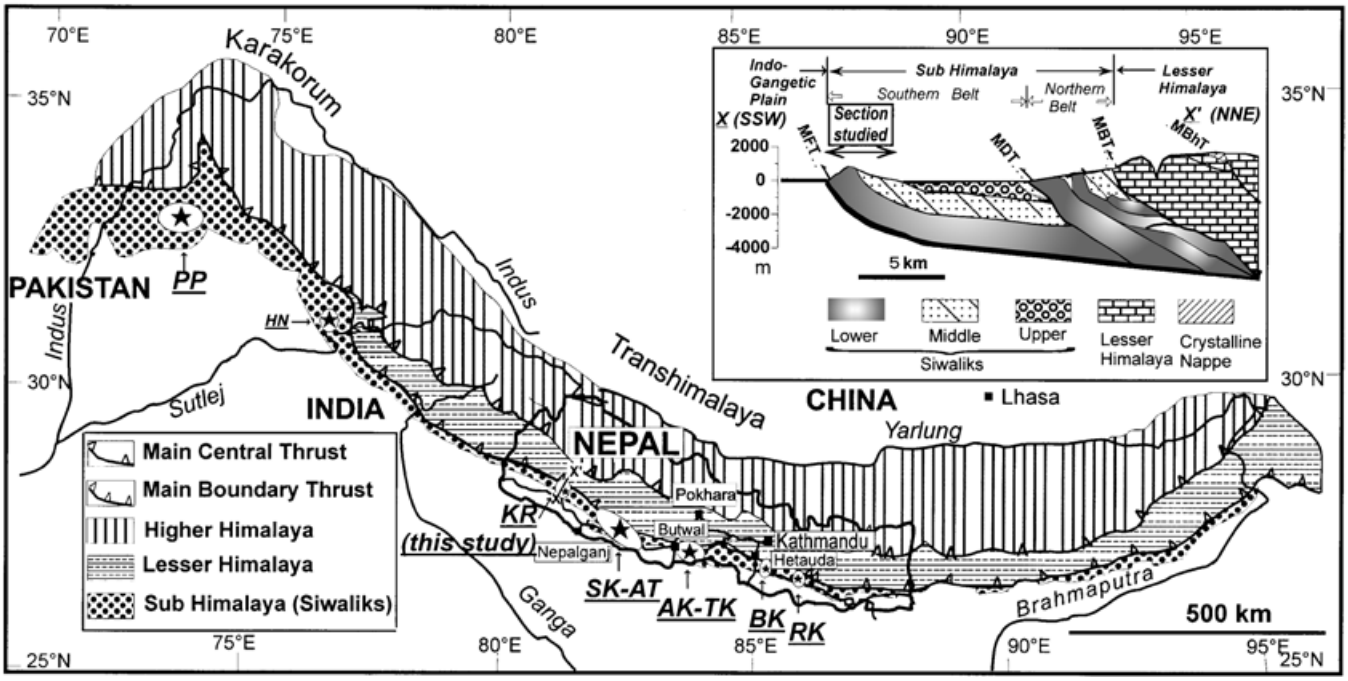

Figure 1. Schematic map of the Himalaya showing the main structural zones (after Gansser 1964). The Karnali River (*KR*) section in western Nepal is shown along with other areas in Nepal where the magnetostratigraphy was studied: *SK–AT* = Surai Khola–Amilia Tui (Appel *et al*. 1991; Rösler *et al*. 1997; Rösler & Appel 1998); *AK–TK* = Arung Khola–Tinau Khola (Tokuoka *et al*. 1986; Gautam & Appel 1994); *BK* = Bakiya Khola (Harrison *et al*. 1993); and *RK* = Rato Khola (Rösler *et al*. 1997). Other locations where the magnetostratigraphy was studied are: *PP* = Potwar Plateau, Pakistan (see Opdyke 1990); and *HN* = Haritalyangar, India (Johnson *et al*. 1983). The inset shows the geotectonic zones along X–X′ parallel to the KR traverse (modified from Mugnier *et al*. 1998).

measured column is part of the >4000 m thick continuous sequence exposed north of Chisapani (28°39′N, 81°17′E) on the East–West Highway in western Nepal (Fig. 1). The results are based on sandstone and siltstone cores collected from 476 levels/sites (Fig. 2b). Preference was given to sandstones/siltstones over clays for several reasons: relatively wider availability throughout the Siwaliks; ease of *in situ* drilling; suitability for thermal demagnetization without the fear of sample destruction; and the proven record of accessible yet consistent characteristic remanent magnetization suitable for magnetostratigraphy (e.g. Tauxe & Badgley 1984, 1988; Friedman *et al*. 1992; Harrison *et al*. 1993; Gautam & Appel 1994; and Rösler & Appel 1998). Rock-magnetic parameters and the magnetic fabric based on the anisotropy of magnetic susceptibility from this sequence have been reported on in Gautam *et al*. (2000).

GEOLOGY AND SAMPLING

The KR gorge has exposed the clastic sediments derived through the erosion of the Himalaya, which underwent episodic uplift following the India–Eurasia collision in Early Tertiary times. Deposition of these sediments into the foreland basin took place during Mio-Pliocene times. Lithologically, they may be divided into Lower Siwaliks (LS), Middle Siwaliks (MS) and Upper Siwaliks (US). Structurally, the region represents a piggy-back imbricate thrust package, which resembles an accretionary prism lying between the Main Frontal Thrust (MFT) and the Main Boundary Thrust (MBT) (Mugnier *et al*. 1998).

According to the section shown in Fig. 1 (inset), the MFT has a steep slope at the surface but becomes shallower with depth until it merges with or transforms to the gently dipping basal decollement at depths of ∼3–4 km—the lower limit of distribution of the alluvial sediments of the Indo-Gangetic Plain. The MBT, also subvertical at the surface but inferred to meet the basal decollement at moderate angles at ∼5 km depth, separates the Mio-Pliocene sediments from the Lesser Himalayan rocks of Precambrian to probably early Neogene age. The foreland basin package may be viewed as a composite of two large-scale sheets separated by another major and extensive, intra-Siwalik, thrust called the Main Dun Thrust (MDT). The southern sheet, about 12 km wide, comprises a continuous sequence of beds dipping consistently north. This sheet encompasses all Siwalik lithologies (LS, MS, US), and its total thickness exceeds 4 km. As in the other sections in central and western Nepal, the Siwalik sediments exhibit an overall upward coarsening trend. The northern sheet, about 6 km wide, is a complex collage of several splays bounded by a set of subordinate thrusts, subparallel at the surface, which merge with the major thrusts at depth.

Sampling was carried out along a 5.6 km long route, with continuous exposures, across the LS and MS lithologies within the southern sheet of the foreland basin sediments. The route starts at the first exposure (28°39.02′N; 81°17.20′E) of fresh green-grey sandstone on the road at the northern end of the Chisapani Bazaar. It ends at the left bank of the KR near its confluence with a tributary flowing from the northeast (opposite a point on the right bank with coordinates 28°42.33′ N and 81°16.53′E) (Fig. 2). Owing to the lack of continuous exposures, a basal part of the LS a few hundred metres thick has not been sampled. Likewise, the uppermost <100 m of the MS sequence, and about 300 m of the US sequence on steep slopes were not sampled due to accessibility problems. The total thickness sampled is calculated to be 3560 m (see the column in Fig. 4). The LS–MS boundary is placed at 2015 m at the base of the

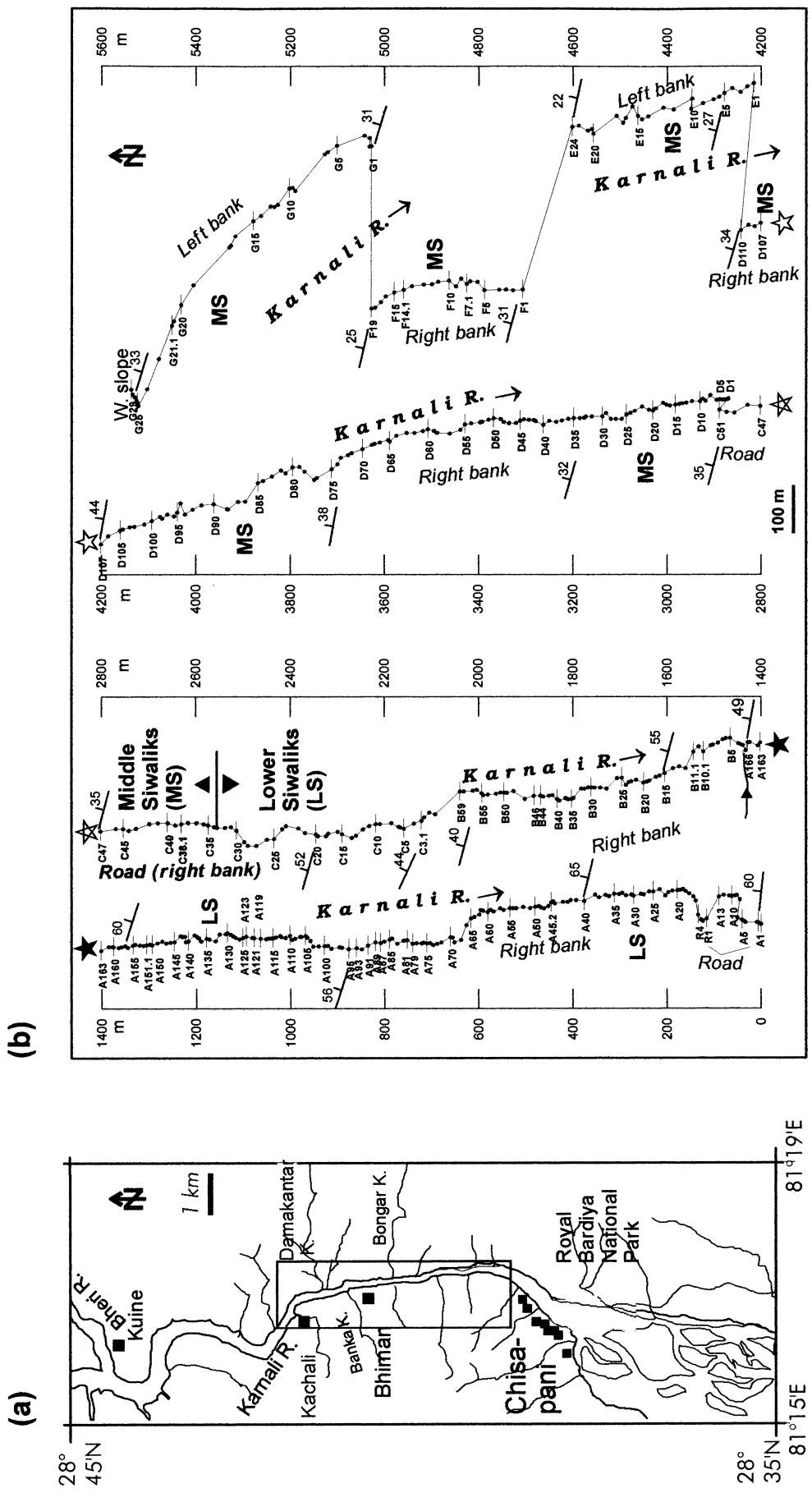

Figure 2. (a) An enlarged view of the KR area studied. (b) The sampling routes along the Karnali River with the locations of the 476 sampling sites/levels indicated. For clarity, only selected sites are labelled.

first prominent bed (>5 m thick) of medium-to-coarse-grained 'salt and pepper' sandstone, following Rösler *et al*. (1997) and Mugnier *et al*. (1998).

The LS sequence is characterized by alternating layers of mainly fine-grained quartzose, partly calcareous sandstones and commonly variegated mudstones. The sandstones are grey in the basal (0–50 m) and upper (1180–2015 m) parts, while they are commonly red and mottled below about 1200 m. Many of the mudstone layers represent oxidized calcitic palaeosols. The thickness of individual sandstone or mudstone bed varies between 0.5 and 5 m, although sandstone beds of 5–12 m, and rarely up to 20 m, thickness are present and their frequency increases stratigraphically upwards. The LS facies were probably mainly deposited by a fine-grained meandering river system (Dhital *et al*. 1995).

The MS lithologies are also represented by alternation of sandstone and mudstone, with the former clearly predominating. The sandstones are generally medium- to coarse-grained, grey, and mica-rich, giving a 'salt and pepper' appearance, whereas the mudstones are mostly non-variegated. The thickness of sandstone beds is typically several metres, but reaches 10–15 m at more than a dozen levels. Even thicker (15–50 m) beds occur at several levels at least. Trough and planar cross laminations are well-developed in sandstones, and channel and scouring structures (up to 300 cm deep) with rip-up clasts are common. Pebble conglomerates intercalated with sandstones appear above 3175 m, following a 50 m thick sandstone bed. Several mudstone layers yield fossil shells and well-preserved plant leaves. Coalified wood remains are common in the middle part (2700–3300 m) in the coarse sandstone beds with or without sand nodules, and a granule-bearing bed at about 2725 m contains vertebrate bone fragments (including teeth). The deposition of the MS facies can be attributed mainly to a sandy braided river system (Ulak & Nakayama 1998).

The US sequence, not sampled here, is represented by gravel beds, with subordinate sand and silt layers, which were possibly formed as alluvial fan deposits near the mountain front. Owing to the dominance of gravel and very coarse sand in the US, it may be difficult to obtain a magnetic polarity sequence with high resolution.

One or two sandstone core samples (2.54 cm in diameter and 6–12 cm in length) were obtained from 476 sites/levels using a portable gasoline-powered drill engine and orientated with a magnetic compass. Sampling localities were divided into seven sections (A, B, D, F on the right bank; C along the road, right bank; and E, G on the left bank) of varying length dictated by the availability of continuous outcrops and accessibility (Fig. 2b). These sections are connected to each other by tracing the beds laterally at their ends. On average, every 8 m of the lithological column has been sampled in order to obtain a high resolution in polarity. The maximum distance between two adjacent sites never exceeds 40 m. In the absence of any significant fault or depositional hiatus, the section may be regarded as continuous. The sedimentary beds have northerly dips varying from $\sim 60^\circ$ to $\sim 20^\circ$ from the southern end to the north (Fig. 2b).

LABORATORY PROCEDURE

Several standard specimens of 2.2–2.4 cm length were cut from these samples in the laboratory, and their remanence and magnetic susceptibility measured. A variety of instruments were employed: a 755R SQUID (2G Enterprizes) magnetometer to measure the remanence of at least one specimen from each level; a static tri-axial demagnetizer of 150 mT capacity (2G Enterprizes) for alternating field demagnetization (AFD); a MMTD60 (Magnetic Measurements) furnace for progressive thermal demagnetization (ThD); a KLY-3 (AGICO) kappa-bridge for measuring low-field susceptibility (k) and its anisotropy; a MMPM9 (Magnetic Measurements) pulse magnetizer with 2.5 T capacity to impart isothermal remanent magnetization (IRM) and a fluxgate spinner magnetometer (Molspin Limited) to measure the IRM acquired after each step of magnetization acquisition; and a SSM-1A spinner magnetometer (Schonstedt) to measure the remanence of 20 IRM-treated specimens. Measurements were carried out at the palaeomagnetic laboratories of the University of Tübingen and Hokkaido University.

NATURAL REMANENT MAGNETIZATION, MAGNETIC SUSCEPTIBILITY AND DEMAGNETIZATION BEHAVIOUR

Results of stepwise AFD up to 150 mT for several specimens are presented in Fig. 3(a). The natural remanent magnetization (NRM) intensity of most fine-grained specimens is almost unaffected (e.g. specimen A37). It may be reduced by less than 50 per cent in some grey fine-to medium-grained sandstones (e.g. specimens B9b, D49a, D89), indicating that a minor fraction of the soft coercivity (<50 mT) remanence resides in maghemite or magnetite. Taking into account the general behaviour of such sediments, at least one specimen per site was subjected to stepwise ThD in progressively higher-temperature steps (usually at 150, 300, 400, 475, 550 and 610 °C).

The variation of the susceptibility, NRM intensity and the ratios of intensities remaining after ThD (at certain temperature steps) with the stratigraphic height are shown in Fig. 4, along with the lithological column. The magnetic susceptibility shows a wider variation, between 10^{-3} and 3×10^{-5} SI units, than the NRM intensity, which is mostly between 10^{-1} and 10 mAm^{-1}. Except for a few specimens with extremely high NRM and magnetic susceptibility, there is no visible correlation between these parameters (Fig. 4). Low-susceptibility values indicate a significant contribution from paramagnetic particles (see Rochette *et al*. 1992). The medium-grained 'salt and pepper' sandstones (MS facies) show high susceptibility ($>10^{-4}$ SI). This is believed to be due to the presence of minor amounts of magnetite (Fe_3O_4) and fairly large amounts of maghemite (γFe_2O_3: the ultimate low-temperature oxidation or weathering product of magnetite), as inferred from the IRM and Curie temperatures (Gautam *et al*. 2000).

The intensity ratios J(150 °C)/J(NRM), J(400 °C)/J(150 °C), and J(610 °C)/J(NRM) are interpreted to be qualitative indicators of the remanence contributed by goethite (αFeOOH), maghemite, and haematite (αFe_2O_3), respectively (Fig. 4). These plots clearly show that the goethite contribution is significant below 1800 m, whereas the opposite is true for maghemite/magnetite. More than 12 per cent of the specimens exhibit J(610 °C)/J(NRM) values lying outside the 0.1–2.0 range, which makes them unlikely to yield the high-blocking-temperature haematite-based detrital remanence.

In general, susceptibility increases stratigraphically upwards, probably owing to the coarsening-upwards nature of the sandstones and the proportional increase in the contribution of

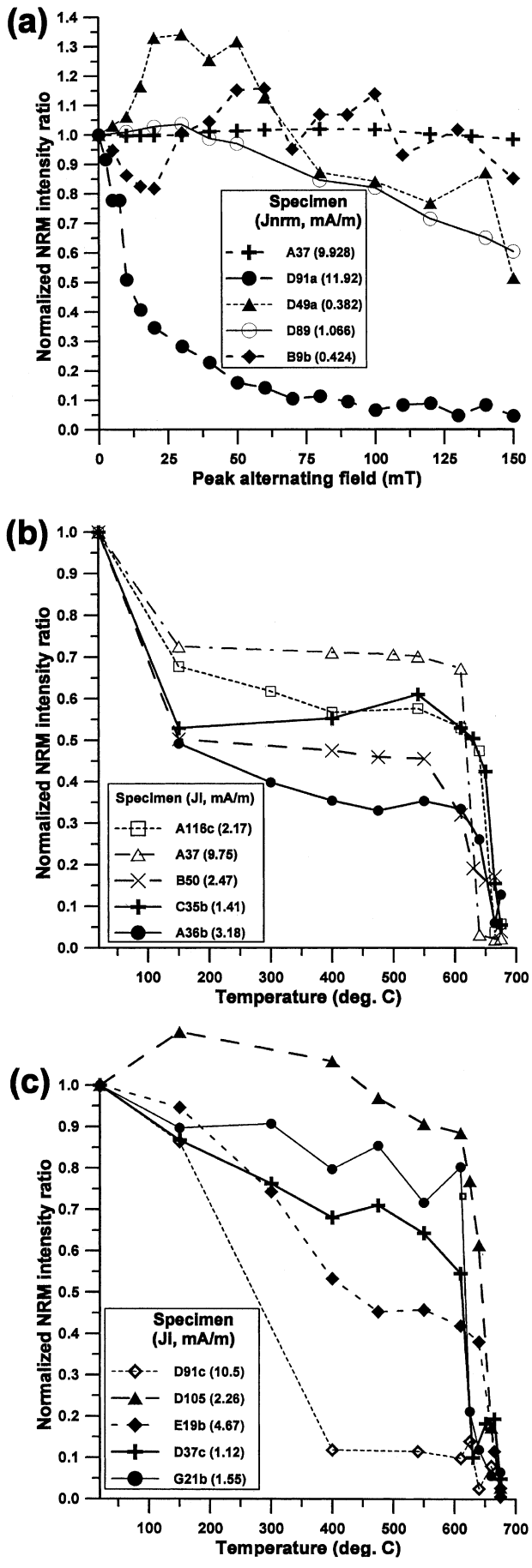

ferrimagnetic minerals (maghemite and magnetite) in the same direction. Judging by the five-point averaged values, the susceptibility changes with stratigraphic height can be divided into three broad segments: (1) the lower segment (below $\sim$1650 m), in which the average k remains mostly below 10^{-4} SI with mean cycles of a few tens of metres; (2) the middle segment (1650–2250 m), in which the average k shows a single 600 m cycle within which the average k fluctuates between 5×10^{-5} and 2×10^{-4} SI; and (3) the upper segment (2250–3560 m), in which the average k remains well above 10^{-4} SI and exhibits cyclic variation (cycles of tens of metres below 2900 m followed by cycles of the order of 100 m above). The lowest susceptibility magnitudes within the middle segment coincide with the marly sandstone beds at several positions (1987–1992 m 1996–1999 m and 2000–2002 m). The anomalous (long-wavelength) susceptibility variation in the middle segment coincides with the period of transition from LS to MS facies and so might be a reflection of the associated long-term climatic change.

The NRM direction commonly shows the presence of a component with a low-unblocking-temperature (T_b) range. This component resides in goethite (resistant to AFD up to 150 mT and $T_b<150$ °C) or maghemite (soft to AFD, $T_b=120$–400 °C), depending on the lithology of the sample. Magnetite (values of T_b up to 400–580 °C) very rarely carries the low-T_b component. The muddy varicoloured specimens affected by a relatively high degree of weathering (LS facies) contain abundant goethite, which contributes up to 90 per cent of the initial NRM. The contribution of maghemite to the remanence is significant in MS lithologies, as seen in the drop of magnetization intensity between 150 and 400 °C.

The direction remaining after ThD at 610 °C is interpreted to reside in haematite (Fe_2O_3), which is consistent with the fact that the remanence is resistant to AFD up to 150 mT. As expected, about 10 per cent of the specimens were dominated by thermally less stable components or had acquired spurious remanence in the laboratory owing to heat-induced production of new magnetic phases, despite the fact that extreme care was taken during demagnetization process.

Figure 3. Normalized intensity response curves showing the behaviour of representative specimens during demagnetization of NRM. (a) AFD curves. Most specimens show irregular response and insignificant (<50 per cent) reduction of the initial NRM, suggesting general ineffectiveness of AFD up to 150 mT (e.g. specimens A37, D49a, D89, B9b). Very few 'salt and pepper' sandstone specimens exhibit the presence of the soft-coercivity remanence shown by specimen D91a. (b) THD curves for specimens (from LS lithologies) showing the predominance of two distinct unblocking temperature (T_b) ranges (low: <150 °C and high: >600 °C). For specimen A37, normalization is done with respect to the remanence left after AFD at 150 mT [see the corresponding curve in (a) above]. The distinct low and high T_b ranges, together with the extreme resistance to AFD, are indicative of the presence of goethite and haematite, respectively. (c) THD curves for specimens (from MS lithologies) showing the presence of two intermediate T_b ranges (lower: 150–400 °C, and upper: 400–600 °C) in addition to the low and/or high T_b ranges. The intermediate T_b ranges are interpreted to reflect the contribution to the remanence by maghemite/magnetite commonly occurring in samples from the upper part (segments D–G). The significant intensity loss within the lower intermediate T_b range exhibited by specimen D91c (diagram c) and the extremely soft nature of the remanence seen in the AFD curve for the sister specimen D91a (diagram a) confirm the contribution of maghemite.

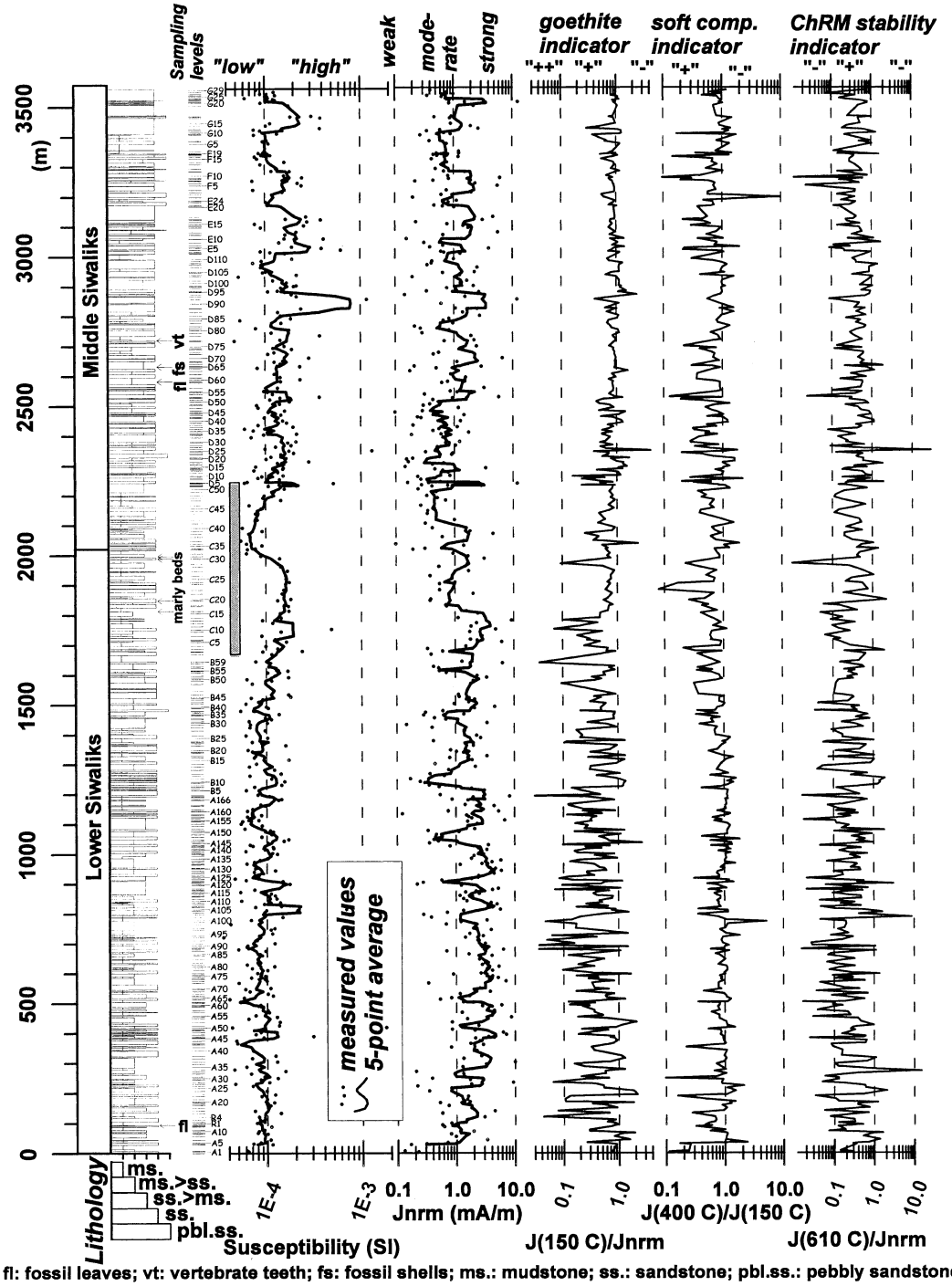

Figure 4. Simplified lithological column, sampling levels and selected rock-magnetic properties versus thickness column. In the log of lithology, the relative length of the horizontal bar corresponds to specific grain size or alternation shown at the base. For clarity, mudstone (clay and siltstone) and sandstone layers are shown individually only if the thickness is at least 4 m; otherwise, they are shown as alternations (mudstone-dominated: ms. > ss. or sandstone-dominated: ss. > ms.). The magnetic susceptibility and natural remanent magnetization intensity J_{nrm} are given together with three intensity ratios: J_{150} °C/J_{nrm}, J_{400}/J_{150} °C, and J_{610} °C/J_{nrm}. These ratios are interpreted as qualitative indictors of the contributions by goethite ('++': very high; '+': moderate to low; '−': almost none), soft-coercivity mineral, basically maghemite ('+': moderate to low; '−': none) and relative stability ('+': stable; '−': unstable) of the high-unblocking-temperature characteristic remanence. The segment between 1650 and 2250 m that represents a single cycle of fluctuation of average susceptibility between 5×10^{-5} and 2×10^{-4} SI is highlighted by the hatched bar.

After analysing the demagnetization behaviour of the specimens treated up to 610 °C, samples showing significant residual intensity at 610 °C but no signs of heat-induced chemical alterations or spurious noise were further treated to ThD up to 675 °C in steps of 10–30 °C. The intensity response of the representative specimens during ThD is shown in Figs 3(b) and (c), where the varying contributions of goethite, maghemite/magnetite and haematite are seen. Stereograms displaying

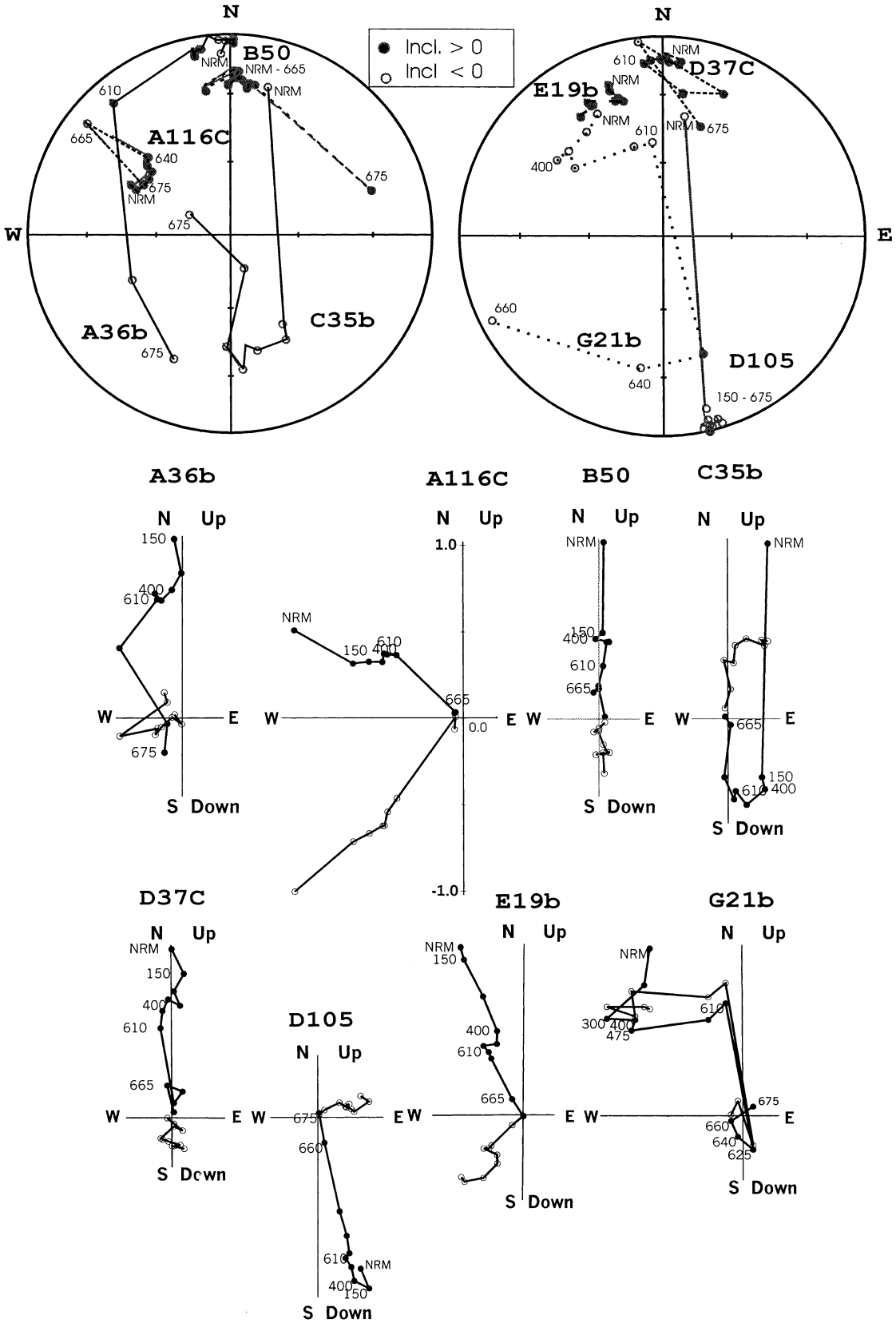

Figure 5. Equal-area projections (upper diagrams) and orthogonal vector plots (lower diagrams) depicting the ThD results of eight specimens considered in Figs 3(b) and (c). Directions are corrected for bedding. Specimens A116c, B50, E19b and D37c exhibit the presence of a stable normal-polarity characteristic remanence (ChRM) persisting to very high temperatures (up to 675 °C) after removal of a component below about 400 °C. Specimens C35b and D105 possess a reverse-polarity ChRM remaining after cleaning a component also at or below about 400 °C. In specimens A36b and G21b, the presence of a reverse-polarity ChRM is indicated by the great-circle trajectories seen at relatively high temperatures (above 400 or even 610 °C), but the stable direction is achieved only at temperatures closer to the Curie temperature of haematite.

the changes in direction after successive demagnetization and the orthogonal vector end-point diagrams are given in Fig. 5. The directions attained well above 610 °C are designated as the characteristic remanence (ChRM) directions. Specimens A116C, B50, D37C and E19b exhibit the presence of stable normal-polarity characteristic remanence (ChRM) which persists to very high temperatures (up to 675 °C) after removal of a low-temperature component below about 400 °C. Specimens C35b and D105 possess a reverse-polarity ChRM which remains after cleaning the low-temperature component, also at or below about 400 °C. In specimens A36b and G21b, the presence of a reverse-polarity ChRM is indicated by the great-circle trajectories seen at relatively high temperatures (above 400 or even 610 °C) but the stable direction is achieved only at temperatures closer to the Curie temperature of haematite.

SUMMARY OF REMANENCE DIRECTIONS

Fig. 6 shows the initial NRM directions of specimens, one from each site. The NRM directions for about half of the specimens show a large bias towards the present-day dipole field (PDF: *in situ* $D/I = 0°/47°$) at the sampling locality. The palaeofield direction for the study area at 10 Ma, the assumed mean age of the KR section, is expected to be about 355°/40° (normal polarity) or 175°/−40° (reverse polarity) after bedding tilt correction from the Indian apparent polar wander path (Klootwijk *et al.* 1985)

The data set obtained by ThD of specimens was analysed using the PALMAG palaeomagnetic program, developed at Munich University, which includes principal component analysis (PCA, Kirschvink 1980) and a remagnetization circle analysis procedure following the algorithm of McFadden & McElhinny (1988).

In most specimens, a normal-polarity component with *in situ* direction close to the PDF, and hence of secondary origin, could be easily recognized in demagnetization trajectories defined by initial temperature steps (<400 °C). As discussed above, the component unblocked below 150 °C was interpreted to reside in goethite, whereas that persisting up to 400 °C was attributed to maghemite. The large bias of the specimen NRM directions towards the PDF seen in Fig. 6 arises as a result of this secondary component. Specimens from 46 sites (i.e. ~10 per cent of the 476 sites sampled) showed the presence of either a secondary PDF-like component [as seen by the drop of J(400 °C) to the practical noise level of the magnetometer] or a totally random demagnetization behaviour.

For the specimens from the remaining 430 sites, the ThD data (for 400 °C and higher-temperature steps) showed the presence of an additional palaeomagnetic direction, which has been already described as a ChRM. In general, some of the following features have been used to identify the ChRM:

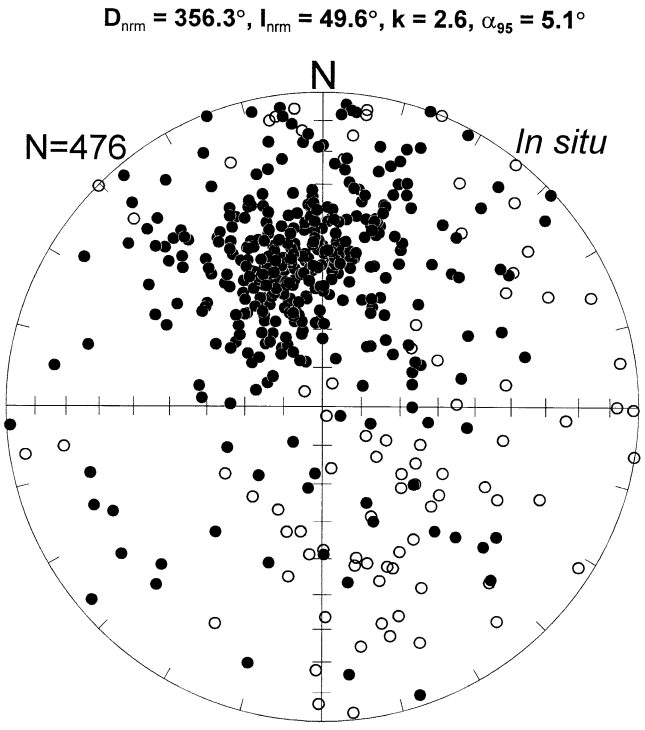

Figure 6. *In situ* NRM directions for all specimens projected in equal-area projection. Note that most of the directions cluster around the present-day field direction ($D = 0°$, $I = 47°$) at the sampling locality (Chisapani: 28°39′N, 81°17′E).

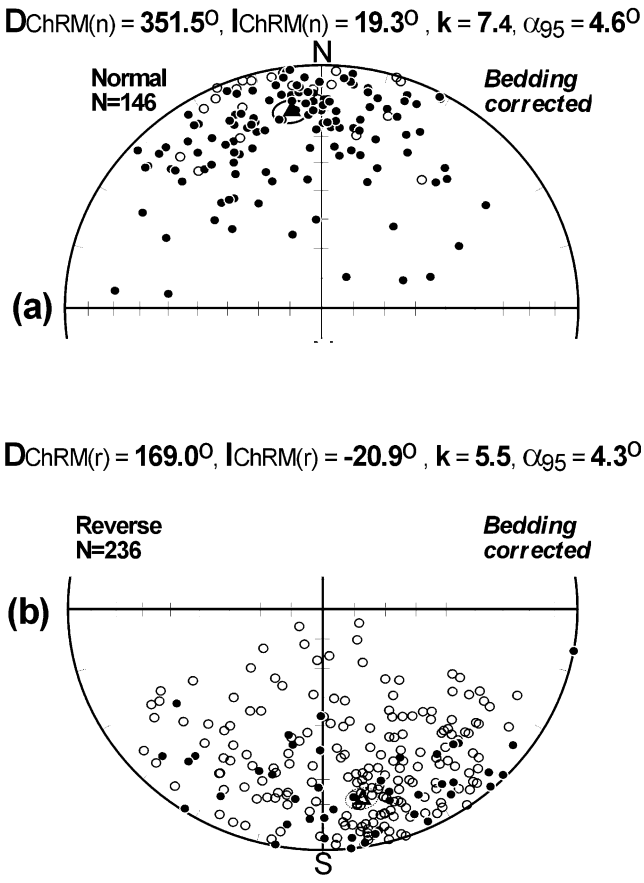

Figure 7. Equal-area projections of bedding-corrected ChRM directions. Normal- and reverse-polarity clusters are shown separately and provided with their mean directions and confidence ellipses calculated using Fisherian statistics. The average inclination of the mean ChRM is about 20° (against an expected 40°−42° inclination), indicating inclination shallowing. The mean declination deviates by 10° (in a counter-clockwise sense) from the present-day north.

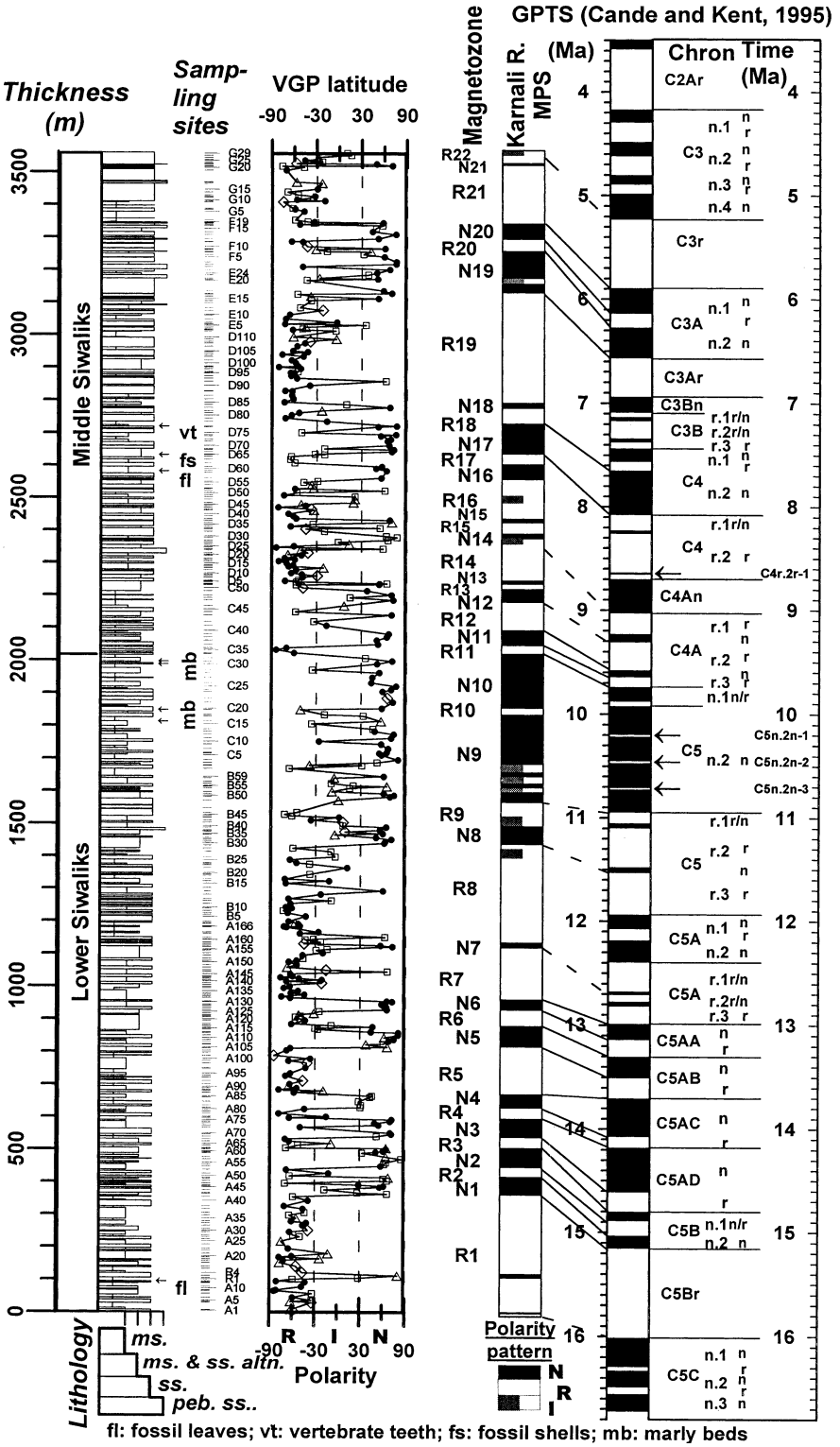

Figure 8. Plot of the VGP latitudes for the sampling levels yielding the ChRM and the inferred MPS for the Karnali River Siwalik sediments. The symbols used in the plots of VGP latitude differ according to the criteria used in ChRM estimates. A solid circle indicates a value based on PCA ('anchored' line fit option; MAD $< 15°$), whereas open symbols (square, triangle and diamond) indicate values based on a selected temperature step (≥ 610 °C, 475 or 525 °C and 400 °C, respectively). Normal (N) and reverse (R) polarities are assigned to sites with VGP latitude of $> +30°$and $< -30°$, respectively. Sites for which the VGP latitude lies between $0° \pm 30°$ are designated as indeterminate (I) polarity. Intervals of normal or reverse polarity determined by two or more adjacent sites are recognized as magnetozones. The resulting MPS consists of 43 magnetozones (R1, N1 ... N21, R22; labelled from bottom to top); it has been correlated with the geomagnetic polarity timescale of Cande & Kent (1995) to assign the depositional ages. The proposed age span for the section is about 10.8 Myr (from 16 Ma to 5.2 Ma), and the boundary between the Lower and Middle Siwaliks falls at about 9.7 Ma.

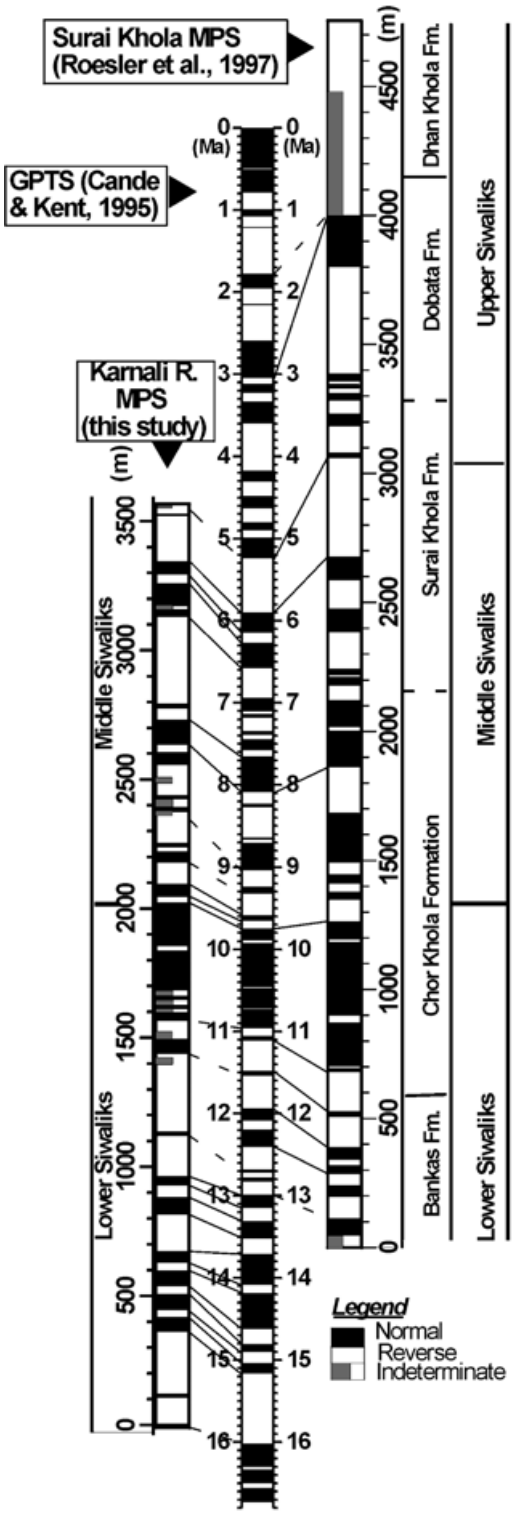

Figure 9. Chronological correlation of the KR section with the Surai Khola (SK) section on the basis of the magnetic polarity stratigraphy. Owing to the differences in the lithological criteria for the formation level boundaries and also the differences in thickness estimates of the SK section appearing in the published literature, it is difficult to assign the stratigraphic positions of such boundaries uniquely. The boundary between Chor Khola and SK Formations corresponds to the base of the thick sandstone bed at the Kaila Khola (Corvinus 1993). The boundary between Dobatta and Dhan Khola Formations is placed at the base of the very thick conglomerate occurring to the NW of the Dhan Khola bridge (Dhital *et al.* 1995).

(1) a stable direction persists to very high temperatures, as indicated by a straight line directed towards the origin in the orthogonal vector plots;

(2) in an equal-area projection diagram, series of points form tightly grouped clusters or show gradual movement of the remanence towards a stable end-point;

(3) in specimens exhibiting acquisition of spurious remanence at or above a certain temperature step, the data points obtained at steps below such a temperature define great circles which converge to the stable end-points mentioned in (2); and

(4) after bedding tilt correction, the direction derived from the straight-line segment or the stable end-point has a declination close to that of the expected normal or reverse palaeofield direction and a shallow to moderate positive or negative inclination.

Actual estimates of the ChRM were first made using the PCA ('anchored' line fit option). This method yielded well-defined ChRM directions (maximum angular deviation $<15^\circ$) in 245 sites. For the remaining 185 sites, the direction reached at a single temperature step, which was judged as the highest possible from the closeness of the achieved direction to the expected stable end-point and also the lack of acquired spurious magnetization, was accepted as the estimate of ChRM. The numbers of sites and the corresponding temperatures used in such a way were 114 ($\geq$610 °C), 47 (475 °C or 525 °C), and 24 (400 °C).

It should be noted here that some of the ChRM directions based on a selected temperature (>400 °C) step may not be free from partial chemical remagnetization, residing in pigmentary haematite, acquired at any time after deposition as a result of alterations, precipitation from solutions or grain-scale tectonic remobilization. Rösler *et al.* (1997) have noted that it is impossible to separate high-blocking-temperature components contributing to such complex remanence in samples (termed 'problematic', say) that are prone to heat-induced chemical changes of iron minerals leading to the production of new magnetic phases in the laboratory.

Polarity identification is based on the sign and value of the latitude of the calculated virtual geomagnetic pole (VGP) (normal: 90° to 30°; reverse: −30° to −90°; indeterminate: −30° to 30°). According to such criteria, 48 sites are designated as of indeterminate polarity, and the remaining 382 sites yield normal or reverse polarities with the following Fisherian statistics:

Normal sites/levels: $N=146$, $D=351.5^\circ$, $I=19.3^\circ$, $k=7.4$, $\alpha_{95}=4.6^\circ$.

Reverse sites/levels: $N=236$, $D=169.0^\circ$, $I=-20.9^\circ$, $k=5.5$, $\alpha_{95}=4.3^\circ$.

The ChRM directions are shown in Fig. 7. The ChRM passes the reversal test. When compared with the expected palaeofield direction (D/I: 355°/40° or 175°/−40°), the mean inclinations are shallower by about 20° while the mean declination deviates to the west by ~5°. The inclination shallowing may be taken as evidence of the largely primary depositional/detrital origin of the remanence (see Tauxe & Kent 1984; Gautam & Appel 1994). The declination anomaly represents a minor counter-clockwise rotation of the Karnali area since the remanence acquisition, but establishing its regional or local nature requires either detailed areal mapping of the geological structures or determination of the magnetic

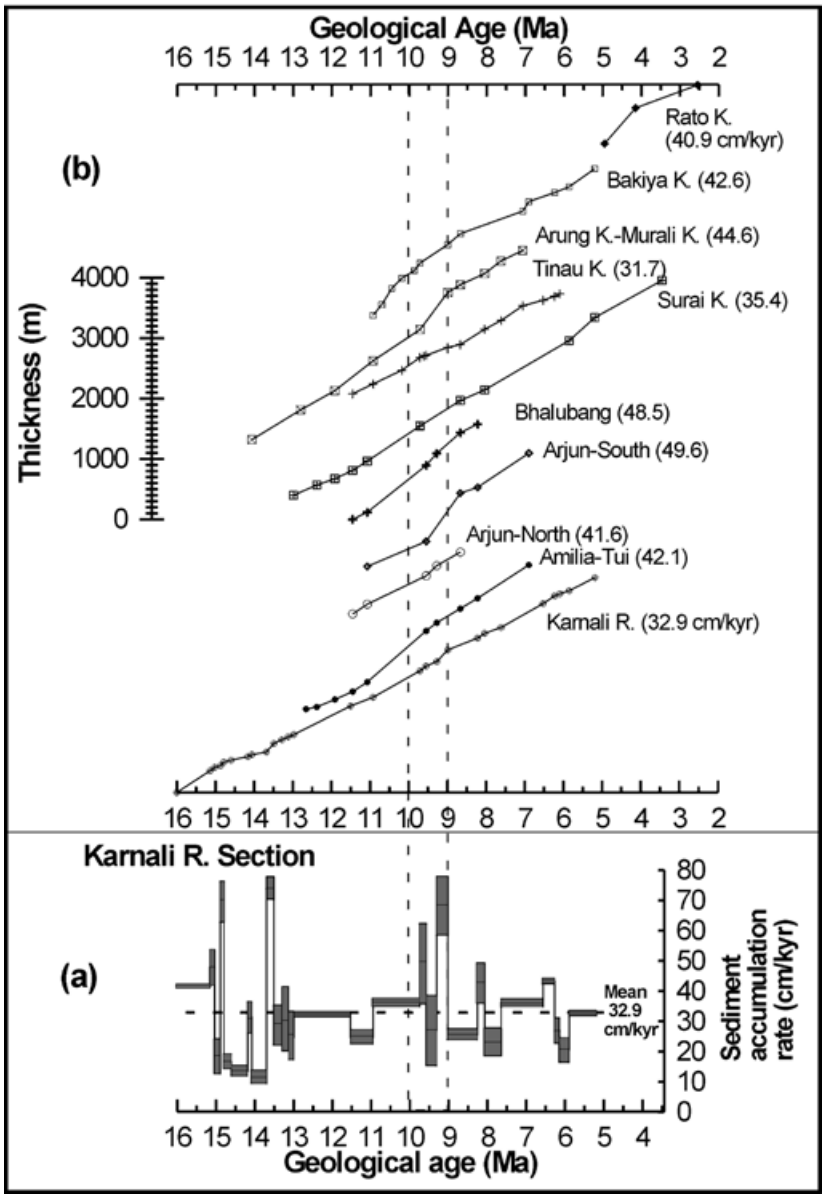

Figure 10. (a) Changes in the sediment accumulation rate (SAR) for the KR section based on the polarity stratigraphy obtained in this study. The height levels, given with shaded boxes of uncertainty, reflect the SAR estimates averaged over the time span covered by their base. (b) Comparison of the sediment accumulation curve for the KR section with similar curves for other sections from the Nepalese Siwaliks (modified from Gautam & Rösler 1999; for data sources of respective sections, refer to caption of Fig. 1). The slope of the curve is proportional to the accumulation rate. The number following the section name gives the average rate for the time span covered by that particular section. The period between 10 and 9 Ma is marked by the highest SARs in most sections of the Nepalese foreland basin.

polarity stratigraphy in additional sections. In general, it is assumed that the characteristic remanence (ChRM) in most specimens represents a depositional remanent magnetization (DRM), although it may not be completely free from a contribution from a post-depositional or even chemical remanence in certain 'problematic' specimens as discussed above.

MAGNETIC POLARITY STRATIGRAPHY AND AGE DATING

The magnetic polarity sequence (MPS) based on the ChRM directions is presented in Fig. 8. Intervals of similar polarity supported by two or more adjacent sites are designated as magnetozones. In order to assign an age range to the MPS, the geomagnetic polarity timescale of Cande & Kent (1995) (CK95) has been used. The CK95 timescale was used for two reasons: (1) it is based on a completely new compilation of relative anomaly spacings using worldwide marine magnetic profiles and chron boundaries that are in line with existing astronomical calibrations; and (2) all published magnetic polarity data from the central sector of the Nepalese Sub-Himalaya have been calibrated to this scale (Gautam & Rösler 1999).

Unfortunately, there are no independent fossil-constrained or isotope-based ages from the section considered. This is also true for other Siwalik sections in Nepal. Likewise, direct lithological correlations of the Nepalese sections with the distant

but magnetostratigraphically well-dated sections in India and Pakistan are not justified due to the prominent lateral variations of these alluvial sediments and the time-transgressive nature of the boundaries even within the sections in Pakistan (e.g. Barry *et al.* 1980). Therefore, the proposed correlation is based solely on matching of the polarity patterns.

At first glance, the Karnali River MPS contains a somewhat higher number of reverse polarity intervals (ratio of normal to reverse polarity sites = 0.62) than expected from the CK95. The fact that this contrasts with data from other well-studied sections such as the Surai Khola and Tinau Khola (see Fig. 1), which yield almost equal numbers of normal- and reverse-polarity sites, may be noted but no explanation can be given at this stage. However, relatively well-defined thick intervals dominated by a single polarity at 0–357 m, 1575–2001 m and 3330–3560 m match with chrons C5Br, C5n and C3r, respectively, and thus facilitate the correlation. Further correlation takes into account the thicknesses of the individual magnetozones and the duration of the polarity chrons to which they are correlated. The frequency of reversals is also considered. As such a correlation procedure is not straightforward, there are uncertainties in the correlation of certain boundaries.

From the correlation proposed in Fig. 8, the Karnali River (KR) section is assigned an age span of 10.8 Myr, from 16 Ma to 5.2 Ma. The use of the revised timescale of Huestis & Acton (1997) for correlation does not change this age range at all; the individual reversal boundaries, however, do change by varying amounts, the maximum shift being $\sim$0.26 Ma (towards the older age) for the reversal boundary between C5An.2n and C5Ar.

Fig. 9 shows the correlation of the KR section (this study) and the Surai Khola section, the longest and best-studied section in Nepal, documented by Rösler *et al.* (1997) in their chronological calibration to the CK95. As noted by Rösler *et al.* (1997), the LS–MS boundary, placed at the onset of thick bodies of 'salt and pepper' sandstone, falls close to the younger limit of chron 5 in most of the Nepalese sections. In the KR section, the LS–MS boundary falls close to 9.7 Ma whereas the MS–US boundary, which falls slightly above the top of the section studied, should be slightly younger than 5.2 Ma. These ages are in agreement with the 9.6 Ma and 5.2 Ma assigned to the LS–MS and MS–US boundaries in the Surai Khola section. The $\sim$1650 m thickness of the MS sequence in the KR section is comparable with that in the Surai Khola section (1720 m). From these observations, we believe that the proposed correlation is reasonable.

SEDIMENT ACCUMULATION RATES

Fig. 10(a) shows the sediment accumulation rates (SAR) together with the uncertainties arising from the locations of the reversal boundaries for the KR section. In order to compare the derived rates with those from other sections in the Nepalese Siwaliks, a summary of the sediment accumulation is given in Fig. 10(b). Average SAR values vary from 32 to 50 cm kyr^{-1}. Values of SAR for sections with a short age range, confined to the middle Siwaliks, exceed 45 cm kyr^{-1}, whereas sections covering a broad age range and both LS and MS lithologies usually yield values below 40 cm kyr^{-1}. Rapid SARs may point to the increase in the rate of tectonic loading by crustal thickening in the hinterland as well as the rate of subsidence of the foreland. Frequent variations in SARs for the KR section (Fig. 10a) and for other Siwalik sections seen in the accumulation curves (Fig. 10b), although not necessarily synchronous in all sections within short timescales, support the episodic nature of such tectonic processes (Harrison *et al.* 1993). The highest SARs seem to be centred at 10–9 Ma in most sections. This time interval may be related to the deepest level of erosion of the crystalline thrust sheets, commencing with the growth of the Lesser Himalayan duplex after $\sim$11 Ma in western Nepal (Decelles *et al.* 1998). For central Nepal, this interval coincides with the beginning of the early Late Miocene (10–7.5 Ma) period of out-of-sequence thrusting within the Lesser Himalaya suggested by Arita *et al.* (1997).

The beginning of the maximum sediment accumulation phase coincides with the time of drastic changes in susceptibility (see Fig. 4 and discussion above). This interval also includes the $\sim$9.5 Ma event of major faunal turnover suggested in the Pakistani Siwaliks, where the biostratigraphic record correlates closely to climatic, oceanographic, and tectonic events, which probably influenced the immigration of the fauna into southern Asia (Barry *et al.* 1985).

ACKNOWLEDGMENTS

We thank E. Appel for allowing us to use the laboratory facilities at the University of Tübingen. We are indebted to K. R. Regmi and D. R. Khadka for their assistance during fieldwork in the Karnali area. We also thank J.-L. Mugnier and H. Pascale of the University of Grenoble for introducing us to the Karnali section and providing geological information. Our sincere thanks go to Nina G. Jablonski of the California Academy of Sciences for kindly reading the manuscript and suggesting linguistic improvements. We gratefully acknowledge the Japan Society for Promotion of Science (JSPS) invitational fellowship awarded for PG's research stay at Hokkaido University.

REFERENCES

Appel, E., Rösler, W. & Corvinus, G., 1991. Magnetostratigraphy of the Miocene–Pleistocene Surai Khola Siwaliks in west Nepal, *Geophys. J. Int.,* **105,** 191–198.

Arita, K., Dallmeyer, R.D. & Takasu, A., 1997. Tectonothermal evolution of the Lesser Himalaya, Nepal: constraints from ^{40}Ar/^{39}Ar ages from the Kathmandu Nappe, *Island Arc,* **6,** 372–385.

Barndt, J., Johnson, N.M., Johnson, G.D., Opdyke, N.D., Lindsay, E.H., Pilbeam, D. & Tahirkheli, R.A.K., 1978. The magnetic polarity stratigraphy and age of the Siwalik Group near Dhok Pathan village, Potwar Plateau, Pakistan, *Earth planet. Sci. Lett.,* **41,** 355–364.

Barry, J.C., Beherensmeyer, A.K. & Monaghan, M., 1980. A geologic record and biostratigraphic framework for Miocene sediments near Khaur village, northern Pakistan, *Postilla,* **183,** 1–19.

Barry, J.C., Johnson, N.M., Raza, S.M. & Jacobs, L.L., 1985. Neogene mammalian faunal change in southern Asia: correlations with climatic, tectonic, and eustatic events, *Geology,* **13,** 637–640.

Burbank, D.W., Beck, R.A. & Mulder, T., 1996. The Himalayan foreland basin, in *The Tectonic Evolution of Asia,* pp. 149–188, eds Yin, A. & Harrison, M., Cambridge University Press, Cambridge.

Cande, S.C. & Kent, D.V., 1995. Revised calibration of the geomagnetic polarity timescale for the Late Cretaceous and Cenozoic, *J. geophys. Res.,* **100,** 6093–6095.

Corvinus, G., 1993. The Siwalik Group of sediments at Surai Khola in western Nepal and its paleontological record, *J. Nepal geol. Soc.,* **9,** 21–35.

Decelles, P.G., Gehrels, G.E., Quade, J., Ojha, T.P., Kapp, P.A. & Upreti, B.N., 1998. Neogene foreland basin deposits, erosional unroofing, and the kinematic history of the Himalayan fold-thrust belt, western Nepal, *GSA Bull.,* **110,** 2–21.

Dhital, M.R., Gajurel, A.P., Pathak, D., Paudel, L.P. & Kizaki, K., 1995. Geology and structure of the Siwaliks and Lesser Himalaya in the Surai Khola-Bardanda area, mid Western Nepal, *Bull. Dept. Geol., Tribhuvan Univ.,* **4,** 1–70.

Flynn, L.J., Pilbeam, D., Jacobs, L.L., Barry, J.C., Behrensmeyer, A.K. & Kappelman, J.W., 1990. The Siwaliks of Pakistan: time and faunas in a Miocene terrestrial setting, *J. Geology,* **98,** 589–604.

Friedman, R., Gee, J., Tauxe, L., Downing, K. & Lindsay, E., 1992. The magnetostratigraphy of the Chitarwata and lower Vihowa formations of the dera Ghazi Khan area, Pakistan, *Sediment. Geol.,* **81,** 253–268.

Gansser, A., 1964. *Geology of the Himalayas,* Wiley Interscience, London.

Gautam, P. & Appel, E., 1994. Magnetic-polarity stratigraphy of Siwalik Group sediments of Tinau Khola section in west central Nepal, revisited, *Geophys. J. Int.,* **117,** 223–234.

Gautam, P. & Rösler, W., 1999. Depositional chronology and fabric of Siwalik Group sediments in central Nepal from magnetostratigraphy and magnetic anisotropy, in *Geology of the Nepal Himalaya: Recent Advances,* eds LeFort, P. & Upreti, B.N., *J. Asian Earth Sci.,* **17(5–6),** 659–682.

Gautam, P., Hosoi, A., Regmi, K.R., Khadka, D.R. & Fujiwara, Y., 2000. Magnetic minerals and magnetic properties of the Siwalik Group sediments of the Karnali river section in Nepal, *Earth, Planets Space,* **52,** 337–345.

Harrison, T.M., Copeland, P., Hall, S.A., Quade, J., Burner, S., Ojha, T.P. & Kidd, W.S.F., 1993. Isotopic preservation of Himalayan/Tibetan uplift, denudation, and climatic histories in two molasse deposits, *J. Geol.,* **101,** 157–175.

Huestis, S.P. & Acton, G.D., 1997. On the construction of geomagnetic timescales from non-prejudicial treatment of magnetic anomaly data from multiple ridges, *Geophys. J. Int.,* **129,** 176–182.

Johnson, N.M., Opdyke, N.D., Johnson, G.D., Lindsay, E.H. & Tahirkheli, R.A.K., 1982. Magnetic polarity stratigraphy and ages of Siwalik Group rocks of the Potwar Plateau, Pakistan, *Paleogeog. Paleoclimat. Paleoecol.,* **37,** 17–42.

Johnson, G.D., Opdyke, N.D., Tandon, S.K. & Nanda, A.C., 1983. The magnetic polarity stratigraphy of the Siwalik Group at Haritalyangar (India) and a new last appearance datum for Ramapithecus and Sivapithecus in Asia, *Palaeogeog. Palaeoclimat. Palaeoecol.,* **44,** 223–249.

Keller, H.M., Tahirkheli, R.A.K., Mirza, M.A., Johnson, G.D., Johnson, N.M. & Opdyke, N.D., 1977. Magnetic polarity stratigraphy of the Upper Siwalik deposits, Pabbi hills, Pakistan, *Earth planet. Sci. Lett.,* **36,** 187–201.

Kirschvink, J.L., 1980. The least-squares line and plane and the analysis of palaeomagnetic data, *Geophys. J. R. astr. Soc.,* **62,** 699–718.

Klootwijk, C.T., Conaghan, P.J. & Powell, C.McA., 1985. The Himalayan Arc: large-scale continental subduction, oroclinal bending and back-arc spreading, *Earth planet. Sci. Lett.,* **75,** 167–183.

McFadden, P.L. & McElhinny, M.W., 1988. The combined analysis of remagnetization circles and direct observations in palaeomagnetism, *Earth planet. Sci. Lett.,* **87,** 161–172.

Mugnier, J.L., Delcaillau, B., Huyghe, P. & Leturmy, P., 1998. The break-back thrust splay of the Main Dun Thrust (Himalayas of western Nepal): evidence of an intermediate displacement scale between earthquake slip and finite geometry of thrust systems, *J. struct. Geol.,* **20,** 857–864.

Opdyke, N.D., 1990. Magnetic stratigraphy of Cenozoic terrestrial sediments and mammalian dispersal, *J. Geol.,* **98,** 621–637.

Opdyke, N.D., Lindsay, E., Johnson, G.D., Johnson, N.M., Tahirkheli, R.A.K. & Mirza, M.A., 1979. Magnetic polarity stratigraphy and vertebrate paleontology of the Upper Siwalik subgroups of Northern Pakistan, *Paleogeog. Paleoclimat. Paleoecol.,* **27,** 1–34.

Ranga Rao, A., Agarwal, R.P., Sharma, U.N., Bhalla, M.S. & Nanda, A.C., 1988. Magnetic polarity stratigraphy and vertebrate paleontology of the upper Siwalik subgroup of Jammu Hills, India, *Geol. Soc. India J.,* **31,** 361–385.

Rochette, P., Jackson, M. & Aubourg, C., 1992. Rock magnetism and the interpretation of anisotropy of magnetic susceptibility, *Rev. Geophys.,* **30,** 209–226.

Rösler, W. & Appel, E., 1998. Fidelity and time resolution of the magnetostratigraphic record in Siwalik sediments: high-resolution study of a complete polarity transition and evidence for cryptochrons in a Miocene fluviatile section, *Geophys. J. Int.,* **135,** 861–875.

Rösler, W., Metzler, W. & Appel, E., 1997. Neogene magnetic polarity stratigraphy of some fluviatile Siwalik sections, Nepal, *Geophys. J. Int.,* **130,** 89–111.

Tauxe, L. & Badgley, C., 1984. Transition stratigraphy and the problem of remanence lock-in times in the Siwalik red beds, *Geophys. Res. Lett.,* **11,** 611–613.

Tauxe, L. & Badgley, C., 1988. Stratigraphy and remanence acquisition of a palaeomagnetic reversal in alluvial Siwalik rocks of Pakistan, *Sedimentology,* **35,** 697–715.

Tauxe, L. & Kent, D.V., 1984. Properties of a detrital remanence carried by haematite from study of modern river deposits and laboratory redeposition experiments, *Geophys. J. R. astr. Soc.,* **76,** 543–561.

Tauxe, L. & Opdyke, N.D., 1982. A time framework based on magnetostratigraphy for the Siwalik sediments of the Khaur area, northern Pakistan, *Palaeogeog., Palaeoclimat., Palaeoecol.,* **37,** 43–61.

Tokuoka, T., Takayasu, K., Yoshida, M. & Hisatomi, K., 1986. The Churia (Siwalik) Group of the Arung Khola area, West Central Nepal, *Mem. Fac. Sci., Shimane Univ.,* **20,** 135–210.

Ulak, P.D. & Nakayama, K., 1998. Lithostratigraphy and evolution of fluvial style of the Siwalik Group in the Hetauda–Bakiya Khola area, central Nepal, *Bull. Dept. Geol., Tribhuvan Univ.,* **6,** 1–14.